

New Photodiode Responsivity Model for RSS-based VLP

Sander Bastiaens^{*‡}, Willem Raes[†], Nobby Stevens[†], Wout Joseph^{*} and David Plets^{*}

^{*} WAVES, INTEC, Ghent University/imec, Ghent, Belgium

[‡] email: Sander.Bastiaens@UGent.be

[†] DRAMCO, ESAT, KU Leuven, Ghent, Belgium

Abstract—Visible Light Positioning (VLP) might enable auspicious tracking systems, well-suited for low-cost and route-configurable autonomous guided vehicles. Yielding the high accuracy required, necessitates a detailed modelling of a photodiode (PD) receiver’s angular characteristics. Still lacking, current RSS-based VLP systems implicitly cope by measuring and (arbitrarily) fitting the received power - distance relation. Upon PD changeover, a recalibration is needed. In this paper, it is shown that adequately modelling the receiver’s angular dependencies (i.e. the responsivity) obsoletes the calibrating fit. Hereto, a new responsivity model is proposed, which is a function of the square of the incidence angle rather than its cosine. An extensive measurement set highlights that this model better matches the measured angular characteristics. In terms of the coefficient of determination R^2 , the new model outcores the baseline Lambertian and generalised Lambertian responsivity models by 1.64% and 0.17% for a Lambertian-like receiver, and by 133% and 1.24% for a non-Lambertian-resembling receiver.

Index Terms - Visible Light Positioning, VLP, RSS, propagation modelling, responsivity, photodiode

I. INTRODUCTION

New indoor positioning technologies are evaluated, in an ongoing search for localisation systems that empower low-cost automated guided vehicles (AGVs) that are self-driving along any route. Visible Light Positioning (VLP) might be a well-suited technology for this application [1]. It employs a photodiode (PD) or image sensor-based receiver to infer positioning estimates based on signals embedded in the visible light originating from a light-emitting diode (LED) infrastructure. Considering that LEDs both are regarded as the light sources of the future, and that they can simultaneously serve for positioning and illumination, VLP should manage to deliver cost-effective systems.

In stroboscopic/flicker-prone and energy-sensitive applications, usually PD-based VLP is favoured to deliver accurate positioning estimates. In [2], Wang et al. equipped a smartphone with a PD and obtained a 90th percentile root Mean Square Error (rMSE) of approximately 0.9 m in an open-plan office. They do first require performing a set of measurements to fit the *received light intensity* as a function of the LED-receiver distance d . In fact, many works on *received signal strength* (RSS)-based VLP necessitate the use of

an (arbitrary) calibrating fit on the $RSS - d$ relation [1], [3], [4], which in addition increasingly diverges from the measured $RSS - d$ for higher d . The fitting is not only a consequence of not-knowing the radiant power of the involved LEDs, but also of the insufficient (receiver) characterisation of the VLP channel. Despite the discrepancy between infrared (IR) and visible light (VL) propagation [5], VLP systems still generally employ IR models [6]. Recently, several attempts have been made to patch these for use in VLP applications [1], [7].

This paper implicitly evaluates the aptitude of the different VL/IR models for line-of-sight (LOS) VL propagation, by looking at the impact of photodiode changeover. It measures (with the setup of section III) the LOS propagation of two commercial receivers at a large set of 151² locations across a 2D plane, 3 m separated in height from the LED plane. The relation between the received photocurrent contributions from each of the LEDs and the receiver-LED distance is fitted for both PDs using the different VLP propagation models and methods available in literature (detailed in section II-A). Subsequently, a more detailed study into the angular characteristics of the PD receiver (responsivity) is performed (see section IV). This study will propose a new generic, quadratic responsivity model, and will indicate that accounting for the relevant (angular) PD characteristics will spare the effort of recalibration (i.e. curve fitting) in case of photodiode changeover. The model will allow a more accurate localisation, as it more closely matches the measured photocurrent contribution versus distance relation.

II. BACKGROUND

A. Channel Modelling

The dominant VLP channel models in literature are still the IR-propagation models of Kahn et al. [6]. Assuming the channel to be both time-invariant stationary and having a flat frequency characteristic, the propagation can be modelled by a DC channel gain. For strict LOS propagation between a single PD and K incoherent white chip-on-board (COB) LEDs LED_i , $i = 1..K$, with accurately-known coordinates $(x_{S,i}, y_{S,i}, z_{S,i})$, the channel model is briefly described below. It dictates the *received radiant flux/power* P_R as

a function of the *transmitted radiant flux/power* $P_{t,i}$:

$$P_R = \sum_{i=1}^K P_{R,i} = \sum_{i=1}^K P_{t,i} h_c^{(i)} \quad (1)$$

where $P_{R,i}$ are demultiplexable using appropriate (de)modulation techniques [8], [9] and where $h_c^{(i)}$ denotes the DC channel gain ($h_c^{(i)} = 0$, $\psi_i > \psi_C$):

$$h_c^{(i)} = R_E(\phi_i) \cdot \frac{A_R \cdot \cos(\psi_i)}{d_i^2} \cdot T_S(\psi_i) \cdot T_R(\psi_i), \quad \psi_i \leq \psi_C \quad (2)$$

with d_i , A_R , ψ_C , ψ_i , ϕ_i , $R_E(\phi)$ designating respectively the LED-PD distance, the PD's active area, the receiver field of view, the incidence angle from LED_{*i*}, the irradiance angle and LED_{*i*}'s radiation pattern. $R_E(\phi)$ is modelled as an ideal Lambertian radiator (of order $m_i = 1$) with $R_E(\phi) = \left[\frac{m_i + 1}{2\pi} \cos^{m_i}(\phi) \right]_{m_i=1}$. $T_S(\psi)$ and $T_R(\psi)$ represent the receiver's optical filter and concentrator gain respectively.

As Miramirkhani et al. [5] already described the discrepancies between IR and VL propagation, recently addendum models have been published. In [7], it is proposed to generalise the Lambertian order, the optical filter and concentrator gain contributions to:

$$P_{R,i} = \frac{P_{t,i}}{d_i^2} C_{opt,i} G_t(\phi_i) G_R(\psi_i) \quad (3)$$

$C_{opt,i}$ is the optical power constant (includes the influence of A_R and $R_E(0)$), while $G_t(\phi)$ and $G_R(\psi)$ denote the transmitter and receiver gain dependencies. When $G_t(\phi) = \cos^{m_t}(\phi)$ and $G_R(\psi) = \cos^{m_R}(\psi)$, (3) can be interpreted as a generalised Lambertian propagation model. It furthermore reduces to (2) when $m_R = 1$ and $T_S(\psi) = T_R(\psi) = 1$. Kim et al. [7] also proposed a more general form for $G_t(\phi)$ and $G_R(\psi)$, the quantities now equalling:

$$G_t(\phi) = \exp(-\phi^{S_t}/k_t), \quad k_t = \frac{(\phi_{1/2})^{S_t}}{\ln(2)} \quad (4)$$

$$G_R(\psi) = \exp(-\psi^{S_R}/k_R), \quad k_R = \frac{(\psi_{1/2})^{S_R}}{\ln(2)}$$

$G_t(\phi)$ and $G_R(\psi)$ are now a function of a slope constant (S_t/S_R for the LED/PD lens respectively) and a semi-angle ($\phi_{1/2}$ and $\psi_{1/2}$). The $P_{R,i}$ are obtained from the receiver photocurrents $I_{PD,i}$ after accounting for the PD's responsivity $R_P(\psi_i, P_{R,i})$:

$$P_{R,i} = I_{PD,i}/R_P(\psi_i, P_{R,i}) \quad (5)$$

$R_P(\psi_i, P_{R,i})$ is assumed to be independent of $P_{R,i}$ as reverse-biased PIN PDs have an extremely linear $P_{R,i} - I_{PD,i}$ response, whilst $P_{R,i}$ is below saturation. Moreover, the additional angular dependence is also neglected in literature: $R_P(\psi) = R_P(0) = R_P$ in [2], [10]. The propagation models of this section can then be used to infer positioning, when combined with the positioning algorithms discussed next.

B. Positioning

1) *Model-Fingerprinting-based*: Model-fingerprinting-based RSS VLP employs a precomputed propagation map, accounting for the relevant channel characteristics. It holds the RSS values per LED for all locations on a predefined positioning grid. Upon an RSS measurement, the positioning estimate equals the grid position that holds the closest match between the modelled and measured RSS values [11].

2) *Trilateration*: Trilateration-based RSS, in its simplest form, obtains the distances d_i from $P_{R,i}$ (or from $I_{PD,i}$ directly). The d_i are given by inverting a propagation model, which is generally either (2) or (3). Afterwards, the d_i are translated into a location estimate (x_U, y_U, z_U) by means of least-squares solving of the cartesian equation group relating d_i to (x_U, y_U, z_U) i.e. via the well-known matrix formalism (as used in [12]).

C. Channel Models for Positioning

Ideally, all parameters in the described channel models (2) and (3) can be predetermined and are constant per LED and receiver type. In practice however, as a consequence of the channel models diverging from real-life measurements, many works in literature calibrate these parameters per LED. Off-line, on-site measurements serve to fit the $RSS - d$ relation on m (see (2)) or m_R/m_t (in (3)) [3], [4]. Some works even calibrate a (seemingly arbitrary) propagation model as a whole e.g. Wang et al. fit a second order polynomial [2]. The drawback of 'fitting' lies in the recalibration effort needed when either the LED, the PD or the environment parameters change. This paper mainly focusses on receiver changeover, as it provides fundamental insight in the optical channel. Adequately modelling the receiver's angular dependencies, proves both that per-LED fitting is generally not required and that the resulting propagation model better matches the $I_{PD,i} - d_i$ relation. The latter implies that the localisation performance can be improved, when employing an appropriate receiver responsivity model.

III. MEASUREMENT SETUP

To study the extent of the impact of a PD's characteristics on the VLP channel model quality, this paper considers an elementary setup. In a 3.75 m x 3.75 m lab set-up covered with black cloths, $K = 4$ (white), commercial off-the-shelf COB LEDs (LED_{*i*}, $i = 1..K$) are suspended 3 m above the receiver plane. *BXRE-50C3001-D-24* LEDs are intensity modulated as to transmit pulse trains (with current magnitudes $\approx [600, 750, 750, 750]$ (mA)) with frequencies $f_{c,i} = 1/T_{c,i}$, each with a duty cycle $\delta_i = 0.5$ [13]. To demultiplex the contributions of the different LEDs at the receiver side, $f_{c,i}$ are chosen to satisfy: $f_{c,i} = 2^{i-1} f_0$ [8]. f_0 is set to 500 Hz to exceed the flicker threshold. The LED coordinates $(x_{S,i}, y_{S,i}, z_{S,i})$ are accurately known, with $\{z_{S,i}\} = [3.005, 3.015, 2.993, 3.004]$ (m).

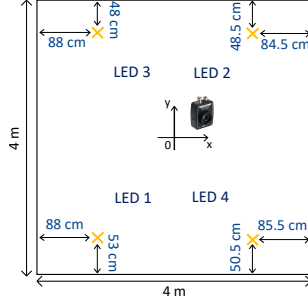


Fig. 1. Bird's eye view of the lab setup

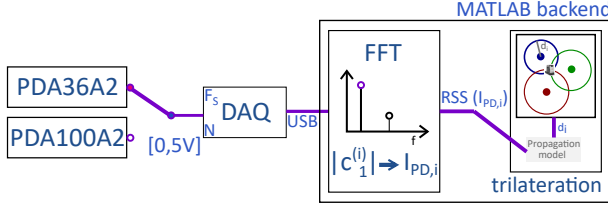


Fig. 2. Schematic representation of the receiver chain

Fig. 1 depicts the LED coordinates and the coordinate system's origin lying in the middle of the room.

This receiver plane is occupied by a commercial photodiode, which is either Thorlabs' PDA100A2¹ or PDA36A2². The characteristics of both photodiodes are listed in Table I. During the measurements, one of either PDs is installed on top of a 2D slider (Velmex' BiSlides) that covers 1 m² with a uniform grid of 41² points. By sequentially displacing the slider 1 m, the entire propagation grid can be measured, with a granularity of 2.5 cm. The photocurrents are digitized using National Instrument's USB-6212 DAQ Device. The DAQ is configured to sample $N = 150$ times at a rate $F_S = 75$ kHz i.e. to ensure coherent sampling. The MATLAB® backend then performs FFT-demodulation into RSS values as specified in [8]. Per measurement location, 10 RSS values are averaged to reduce the noise impact. Fig. 2 depicts the schematic representation of this receiver chain. The changeover of Thorlabs' PDA36A2 to PDA100A2 is studied, as both photodiodes not only differ in form factor (square versus round) and active area A_R , but in wavelength-dependence of their responsivity $R_P(0)$ (A/W) as well.

IV. CHANNEL CHARACTERISATION

In order to both model the receivers' (angular) characteristics and study their impact on $I_{PD,i} - d_i$ (and thus implicitly on the positioning), the propagation is measured across the 2D receiver plane. The receivers' normal n_R is assumed to be equal to $[0\ 0\ 1]$. The (demodulated) received photocurrents $I_{PD,i}$ are shown in Fig. 3, for LED 3 and respectively the (a) PDA36A2 and (b) PDA100A2.

¹ <https://www.thorlabs.com/thorproduct.cfm?partnumber=PDA100A2>

² <https://www.thorlabs.com/thorproduct.cfm?partnumber=PDA36A2>

TABLE I
COMPARISON OF PDA100A2 AND PDA36A2

| PDA100A2 | PDA36A2 |
|---|---|
|  |  |
| Form Factor: Round | Form Factor: Square |
| Active Area: 75.4 mm ² | Active Area: 13 mm ² |
| Gain: $G_t = 4.75 \cdot 10^4$ V/A | Gain $G_t = 4.75 \cdot 10^5$ V/A |
| Retainer Ring: Present | Retainer Ring: Absent |
| Z-coordinate: 0 m | Z-coordinate: -2.5 mm |

A. Calibration

To limit the influence of all non-responsivity channel contributions, an additional calibration is required. A nonnegligible LED tilt is present in the lab setup and needs compensation. When rearranging the terms of (2), for $m = 1$, the most likely tilted LED normal is found where $I_{PD,i} \cdot d_i^3$ is maximal [14]. A more robust method entails not taking the maximum's location, but the $I_{PD,i} \cdot d_i^3$ -weighted centroid of all locations with an $I_{PD,i} \cdot d_i^3$ larger than the 95th percentile of all $I_{PD,i} \cdot d_i^3$. The centroids are highlighted in red in Fig. 3 (c). The tilt is then compensated for by sequentially dividing the measurement data $I_{PD,i}$ on each grid location (x, y) by $\cos(\phi_m(x, y))$ and multiplying it by $\cos(\phi_{id}(x, y)) = (z_{S,i} - h)/d_i(x, y)$. $\phi_m(x, y)$ and h represent the measured irradiance angle (with respect to tilted LED normals $\{n_{S,i}\}$) and the z-coordinate of the PD (see table I).

It also has to be noted that for VL, both the LEDs' radiation pattern $R_E(\phi)$ and the receiver responsivity $R_P(\psi)$ vary with the wavelength λ . Introducing a gain mismatch factor M that accounts for the wavelength mismatch between transmitter and receiver, allows a continuing λ -abstraction. $P_{t,i}$ also requires a calibration, as it is never exactly known without measuring [15]. Given M and $R_P(0)$, $\{P_{t,i}\}$ are calibrated directly beneath each LED. The calibrated $P_{t,i,fit}$ satisfy approximately $P_{t,1,fit} \cdot [1\ 1.245\ 1.225\ 1.2]$. $P_{t,i,fit}|_{i>1} < 1.25 P_{t,1,fit}$ can (partly) be attributed to the LED driving current - $P_{t,i}$ relation starting to saturate (see section III). In addition, the variation in $P_{t,i}$ will impede propagation models that assume a LED independent $P_{t,i,fit} = P_{t,fit}$.

B. Photocurrent $I_{PD,i}$ - distance d_i curve (fitting)

Fig. 4 (a) and (b) depict the (calibrated) measured received photocurrent $I_{PD,4}$ - distance d_4 ($i = 4$) relation in grey dots, respectively for the PDA36A2 and the PDA100A2. It is important to up front note two aspects. First, this curve is only valid for this particular receiver/LED constellation. Second, noise and small measurement/setup errors (e.g. imperfectly compensated tilt) cause the curves to widen with increasing d .

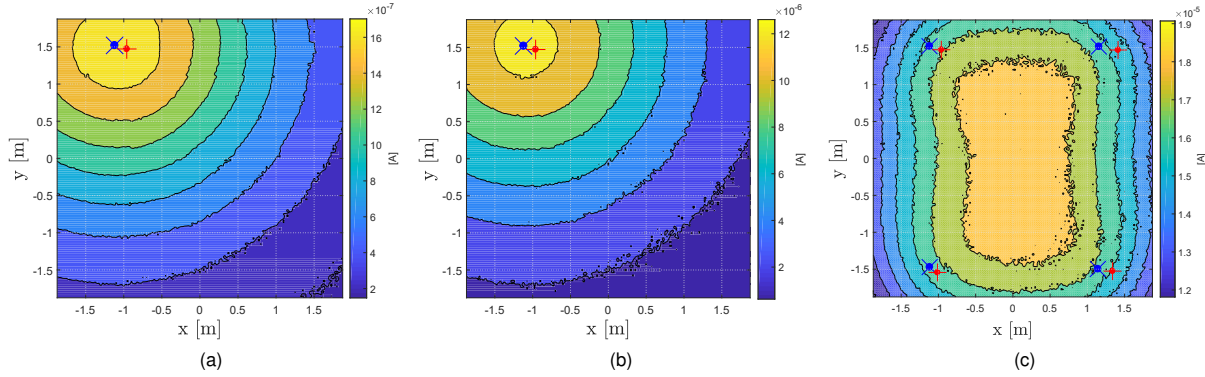


Fig. 3. Distribution of $I_{PD,3}$ measured with the (a) PDA36A2 and (b) PDA100A2 across the receiving plane. (c) plots PDA100A2's $\sum_{i=1}^K I_{PD,i}$, but where all $I_{PD,i}$ are weighted to all have equal $P_{t,i} = P_{t,1}$. The blue markers represent the ground truth LED locations, whereas the red markers highlight the points of incidence between the LEDs' surface normals $\{n_{S,i}\}$ and the ground plane.

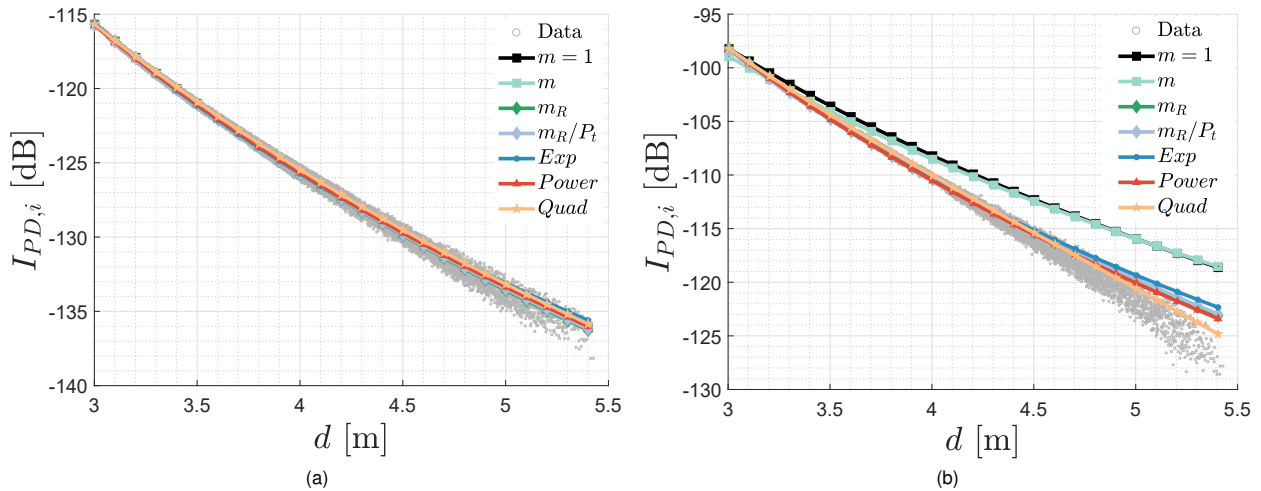


Fig. 4. $I_{PD,i} - d_i$ and the (fitted) propagation models as found in literature for (a) the PDA36A2 and (b) the PDA100A2.

Fig. 4 also explores the various propagation models obtained by effectuating the fitting methods of section II on a per-LED basis. The baseline model of (2) with $P_{t,i,fit}$ is dubbed (i) $m = 1$ and is represented in black. The (ii) m and (iii) m_R model fix $P_{t,i,fit}$ and fit respectively the lambertian order m in (2) and the general lambertian receiver order m_R in (3). Although resembling, the former fits the LED properties, while the latter fits the receiver's i.e. they present a different view on fitting. Adding a degree of freedom, models (iv) m/P_t and (v) m_R/P_t also allow simultaneously fitting $P_{t,i,fit}$ to the measurement data. (vi) Exp determines the best-suited $\psi_{1/2}$ and S_R of (4). (vii) $Power$ employs the curve fitting tool *cftool* of MATLAB® (i.e. nonlinear least squares minimisation) to deliver the best-fitting $I_{PD,i} = f(d_i) = a(d_i)^b$. $Power$ should deliver a model well-suited for trilateration as d_i is easily gathered from $I_{PD,i}$. All model parameters are fit by minimising the rMSE between the modelled and measured data. Each model's mean coefficient of determination R^2 with respect to the measurement data is listed in Table II.

Fig. 4 and Table II allow concluding that the PDA-36A2 exhibits a rather Lambertian-like responsivity behaviour: $R_P(\psi) \sim R_P$. In contrast, the PDA100A2 absolutely does not. This is confirmed by looking at the best-fitted model parameters. The mean cosine powers m , m_R amount to 1.01 and 0.93, while for the PDA100A2 the associated values are 0.87 and 1.76. The mean S_R and $\psi_{1/2}$ equal 2.18/1.11 for PDA36A2 and 2.25/0.82 for PDA100A2. S_R is rather consistent, indicating a more robust model. The mean exponents of the *power* fit are -3.87 and -4.84 i.e. really emphasising the difference between both receiver configurations.

Importantly though, the fitted $I_{PD,i} - d_i$ relations diverge more and more from the measured ones with increasing distance d_i . This behaviour (also treated in section IV-D) will, depending on the VLP roll-out situation, significantly impact the positioning accuracy. The models of this section are fitted per LED, and hence correspond to fitting a practical propagation model in situ [3]. However, modelling the receiver responsivity $R_p(\psi)$ will spare this effort, as is shown hereinbelow.

TABLE II
MEAN COEFFICIENT OF DETERMINATION R^2

| PDA | $m = 1$ | m | m_R | m_R/P_t | Exp | $Power$ |
|-------|---------|-------|-------|-----------|-------|---------|
| 36A2 | 0.997 | 0.998 | 0.999 | 0.999 | 0.998 | 0.999 |
| 100A2 | 0.96 | 0.97 | 0.998 | 0.998 | 0.995 | 0.998 |

C. Responsivity Conventions

As section II-A described, the responsivity $R_P(\psi)$ usually relates $I_{PD,i}$ to $P_{R,i}$ using (5), where $P_{R,i}$ is in itself already dependent on the incident angle ψ_i at the receiver. The following section takes a different approach. It extends the definition of the PD's responsivity $\mathbf{R}_P(\psi)$ to encompass all angular receiver dependencies. Depending on the propagation model, $\mathbf{R}_P(\psi)$ thus includes $R_P \cdot \cos(\psi)$, $R_P \cdot \cos^{m_R}(\psi)$ or $R_P \cdot G_R(\psi)$ in respectively (2), (3), and (4). As both the LEDs and the PDs are not explicitly equipped with a lens, $T_S(\psi)$, $T_R(\psi)$ and $G_t(\phi)$ are equal to 1. Technically, the exponential $G_R(\psi)$ form also describes a lens, but here this ψ -dependence is generalised to a 'responsivity factor'. The subsequent analysis treats the normalised responsivity $\widehat{R}_P(\psi)$, in order to solely focus on the angular dependence of the receiver. $\widehat{R}_P(\psi)$ is derived from $\mathbf{R}_P(\psi)$ by division by the maximum responsivity $R_P(0)$.

D. Responsivity Modelling

Fig. 5 depicts the normalised receiver responsivity $\widehat{R}_P(\psi)$ of both Thorlabs receivers, over the incidence angle ψ . This figure is derived from all LEDs' measurement data, by compensation of $R_E(\phi) = \cos^m(\phi)|_{m=1}$ and d_i , and per LED normalisation. The clear disparity in $\widehat{R}_P(\psi)$ between both receivers can be remarked.

In search for an appropriate receiver responsivity model, the propagation models from the previous section are revisited. However, the set of models should now strictly be perceived as responsivity models and are hence LED independent.

The considered responsivity models are fit on $\widehat{R}_P(\psi)$ and are subsequently depicted in Fig. 5. (i) The Lambertian model $\widehat{R}_P(\psi) = \cos(\psi)$ (named $m = 1$ and visualised in black) yields an R^2 score of 0.975/0.426 for the PDA36A2/PDA100A2. (ii) The generalised Lambertian model $\widehat{R}_P(\psi) = \cos^{m_R}(\psi)$ (dubbed m_R and with $m_R = 0.93/1.84$) improves R^2 to 0.99/0.982. It particularly fits PDA36A2's $\widehat{R}_P(\psi)$ well. (iii) The exponential form of $G_R(\psi)$ (Exp , see (4)), with $S_R = 2.60/2.57$ and $\psi_{1/2} = 1.04/0.80$ rad, is more able to account for the PDA100A2-receiver's behaviour. When $\widehat{R}_P(\psi) \approx 1/2$ is inadequately known (see Fig. 5), Exp may encounter difficulties. (iv) A slightly modified model $Exp^{3/4}$ (with a comparable R^2 score) utilises the "three-quarter" angle $\psi_{3/4}$ instead of the semi-angle $\psi_{1/2}$: $\widehat{R}_P(\psi) = \exp(-\psi^{S_R}/\psi_{3/4}^{S_R} \ln(4/3))$ with $S_R = 2.37/2.72$ and $\psi_{3/4} = 0.74/0.58$ (rad). (v) Again, a

TABLE III
COEFFICIENT OF DETERMINATION R^2 RESPONSIVITY

| PDA | $m = 1$ | m_R | Exp | $Exp^{3/4}$ | $Quad$ | Opt |
|-------|---------|-------|-------|-------------|--------|-------|
| 36A2 | 0.975 | 0.99 | 0.987 | 0.99 | 0.991 | 0.992 |
| 100A2 | 0.426 | 0.982 | 0.989 | 0.988 | 0.995 | 0.996 |

more suited model Opt is proposed: by employing $cftool$: $\widehat{R}_P(\psi) = 1 - a \cdot \psi^b$. With $a = 0.46/0.77$ and $b = 2.11/2.02$, the R^2 score is pushed to 0.992 and 0.996 respectively. Given that $b \sim 2$ and based on the above insights, this paper proposes a new quadratic (vi) $\widehat{R}_P(\psi)$ model, named $Quad$:

$$\widehat{R}_P(\psi) = \begin{cases} 1 - \frac{\psi^2}{(\psi_{3dB})^2} \cdot \frac{\sqrt{2}-1}{\sqrt{2}}, & |\psi| \leq |\psi_C| \\ 0, & |\psi| > |\psi_C| \end{cases} \quad (6)$$

in which ψ_{3dB} represents the ψ for which $\widehat{R}_P(\psi) = 1/\sqrt{2}$ (i.e. a 3 dB electrical power decrease). $|\psi_C|$ equals $\sqrt{\frac{\sqrt{2}}{\sqrt{2}-1}} \cdot \psi_{3dB}^2$. Rated at $R^2 = 0.991/0.995$, $Quad$ well-approximates the Opt fit (with $\psi_{3dB} = 0.81/0.62$ (rad)), as well as exceedingly outperforms the m_R model. The models' resulting coefficients of determination are collected in Table III. In terms of relative R^2 scores, $Quad$ manages a 1.64%/0.17% (PDA36A2) and 133%/1.24% (PDA100A2) increase in aptitude to model the measured $\widehat{R}_P(\psi)$, when compared to both the baseline $m = 1$ and generalised Lambertian m_R model. As $Quad$ outscores the traditional $\widehat{R}_P(\psi)$ models in terms of the goodness of fit, employing $Quad$ in e.g. model-fingerprinting-based RSS [11] will improve the localisation accuracy.

It can be remarked that all $\widehat{R}_P(\psi)$ models increasingly diverge from the measured data, for larger ψ . This results from inherent photodiode physics, packaging and Fresnel losses. The latter manifest at higher ψ and are out of scope.

E. Receiver Changeover

Upon receiver changeover, the models of section IV-B all require refitting. A dedicated receiver model, as proposed in the previous section IV-D, should remove the need for this recalibration. To justify the latter, employing a $\widehat{R}_P(\psi)$ responsivity model should result in R^2 scores that rival those listed in Table II. Computing the R^2 values of the $Quad$ -based propagation model:

$$I_{PD,i} = \frac{P_{t,i,fit} \cdot R_E(\phi_i) \cdot A_R}{d_i^2} \cdot \mathbf{R}_P(\psi_i) \quad (7)$$

returns 0.9981/0.9984 for the PDA36A2/PDA100A2. Both values translate into a relative R^2 score improvement of 0.07% and 4.03% over the baseline model. Model (7), $Quad$ in Fig. 4, matches the m_R propagation model of section IV-B in its aptitude to represent the measured $I_{PD,i} - d_i$. The R^2 scores differ less than

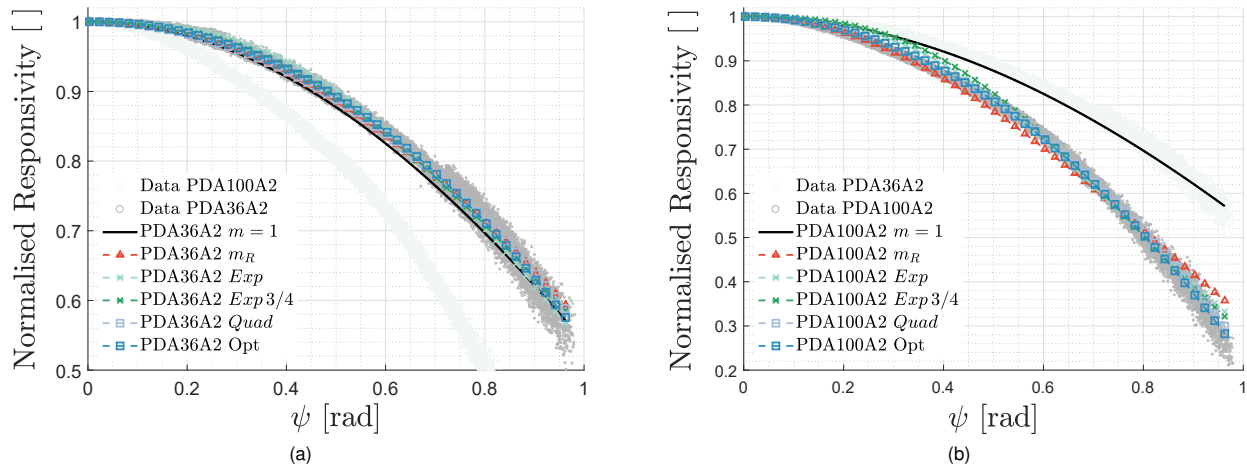


Fig. 5. Measured normalised responsivity curves and $\widehat{R}_P(\psi)$ models with an emphasis on (a) the PDA36A2 and (b) the PDA100A2.

0.1%, despite the latter fitting all $I_{PD,i} - d_i$ curves individually per LED. The above allows to conclude that upon PD changeover, it suffices to swap the $\widehat{R}_P(\psi)$ model and accurate positioning will be maintained.

V. CONCLUSION AND FUTURE WORK

This work investigates the influence of a photodiode receiver's angular dependence $\widehat{R}_P(\psi)$ on the relation between the photocurrent contribution $I_{PD,i}$ and the receiver-transmitter distance d_i . Whereas in literature RSS-based VLP systems are only able to ensure accurate localisation through (arbitrarily) fitting $I_{PD,i} - d_i$ per LED, this paper shows that adequately modelling $\widehat{R}_P(\psi)$ via *Quad*, a proposed function of the square of the incidence angle ψ rather than its cosine, obsoletes this calibrating fit. In modelling $\widehat{R}_P(\psi)$ itself, *Quad* ameliorates the relative R^2 with respect to the baseline cosine model score with 1.64% and 133% for a Lambertian-like and non-Lambertian-like receiver.

The future work is miscellaneous. More aspects of $\widehat{R}_P(\psi)$ need to be investigated e.g. studying the impact of $\widehat{R}_P(\psi)$ on the positioning, reconciling a noninvertible *Quad* with trilateration and incorporating Fresnel losses. Importantly, this work provides a first step towards VLP proprietary (i.a. non-line-of-sight) propagation models.

VI. ACKNOWLEDGMENT

This work was performed within LEDsTrack, a project co-financed by imec and receiving project support from *Flanders Innovation & Entrepreneurship*.

REFERENCES

- [1] Y. Zhuang et al., "A Survey of Positioning Systems Using Visible LED Lights," in *IEEE Communications Surveys & Tutorials*, vol. 20, no. 3, pp. 1963-1988, 2018.
- [2] Q. Wang et al., "Light positioning: A high-accuracy visible light indoor positioning system based on attitude identification and propagation model," in *International Journal of Distributed Sensor Networks*, vol. 14, no. 2, pp 1-13, 2018.
- [3] F. Alam, M. T. Chew, T. Wenge and G. S. Gupta, "An Accurate Visible Light Positioning System Using Regenerated Fingerprint Database Based on Calibrated Propagation Model," in *IEEE Transactions on Instrumentation and Measurement*, early access.
- [4] H. Zheng, Z. Xu, C. Yu and M. Gurusamy, "A 3-D high accuracy positioning system based on visible light communication with novel positioning algorithm," in *Optics Communications*, vol. 396, pp. 160-168, 2017.
- [5] F. Miramirkhani and M. Uysal, "Channel Modeling and Characterization for Visible Light Communications," in *IEEE Photonics Journal*, vol. 7, no. 6, pp 1-16, 2015.
- [6] J. M. Kahn and J. R. Barry, "Wireless infrared communications," in *Proceedings of the IEEE*, vol. 85, no. 2, pp. 265-298, 1997.
- [7] H. Kim, D. Kim, S. Yang, Y. Son and S. Han, "An Indoor Visible Light Communication Positioning System Using a RF Carrier Allocation Technique," in *Journal of Lightwave Technology*, vol. 31, no. 1, pp. 134-144, 2013.
- [8] S. De Lausnay, L. De Strycker, J. P. Goemaere, N. Stevens and B. Nauwelaers, "A Visible Light Positioning system using Frequency Division Multiple Access with square waves," *International Conference on Signal Processing and Communication Systems*, pp. 1-7, 2015.
- [9] H. Steendam, "A 3-D Positioning Algorithm for AOA-Based VLP With an Aperture-Based Receiver," in *IEEE Journal on Selected Areas in Communications*, vol. 36, no. 1, 2018, pp. 23-33.
- [10] H. Chen, W. Guan, S. Li and Y. Wu, "Indoor high precision three-dimensional positioning system based on visible light communication using modified genetic algorithm," *Optics Communications*, vol. 413, pp. 103-120, 2018.
- [11] S. Bastiaens, D. Plets, L. Martens and W. Joseph, "Response Adaptive Modelling for Reducing the Storage and Computation of RSS-based VLP," *International Conference on Indoor Positioning and Indoor Navigation*, pp. 1-7, 2018.
- [12] W. Gu, M. Aminikashani, P. Deng and M. Kavehrad, "Impact of Multipath Reflections on the Performance of Indoor Visible Light Positioning Systems," in *Journal of Lightwave Technology*, vol. 34, no. 10, pp 2578-2587, 2016.
- [13] W. Raes, L. De Strycker and N. Stevens, "Design and Accuracy Evaluation of a RSS-Based Visible Light Positioning Implementation," *Workshop on Positioning, Navigation and Communications*, pp. 1-5, 2018.
- [14] D. Plets, S. Bastiaens, L. Martens, W. Joseph, "An Analysis of the Impact of LED Tilt on Visible Light Positioning Accuracy," in *Electronics 2019*, vol. 8, no. 4, 389, 2019.
- [15] D. Plets, S. Bastiaens, N. Stevens, L. Martens, W. Joseph, "Monte-Carlo simulation of the impact of LED power uncertainty on visible light positioning accuracy," *International Symposium on Communication Systems, Networks Digital Signal Processing*, pp. 589-594, 2018.